Highly Luminescent Covalently Linked Silicon Nanocrystal/Polystyrene Hybrid Functional Materials: Synthesis, Properties, and Processability

*Zhenyu Yang, Mita Dasog, Alexander R. Dobbie, Ross Lockwood, Yanyan Zhi, Al Meldrum, and Jonathan G. C. Veinot**

Silicon nanocrystals (SiNCs) have received much attention because of their exquisitely tunable photoluminescent response, biocompatibility, and the promise that they may supplant their CdSe quantum dot counterparts in many practical applications. One attractive strategy that promises to extend and even enhance the utility of SiNCs is their incorporation into NC/polymer hybrids. Unfortunately, methods employed to prepare hybrid materials of this type from traditional compound semiconductor (e.g., CdSe) quantum dots are not directly transferable to SiNCs because of stark differences in surface chemistry. Herein, the preparation of chemically resistant SiNC/polystyrene hybrids exhibiting exquisitely tunable photoluminescence is reported and material processability is demonstrated by preparing micro and nanoscale architectures.

1. Introduction

Semiconductor nanocrystals, or quantum dots (QDs), and functional polymers are among the many triumphs of modern materials chemistry.[1–4] QDs of a vast array of compound semiconductors (e.g., CdSe, CdS, PbSe) are now routinely prepared and exploited for their size-dependent optical, electronic, and chemical properties.[5–8] Similarly, synthetic advances in polymer chemistry now allow rational design and tailoring of their material characteristics.[9–12] Marrying the exquisitely tunable properties of these two very different materials to produce hybrids offers yet another degree of freedom in the preparation of designer materials that find application in far reaching areas including optoelectronic structures,[4,13] drug delivery systems,[14] sensors,[15] solar cells,[16] LEDs,[10] and data storage.[17]

Still, hurdles associated with the development of these hybrids remain that could slow and even preclude their practical implementation. Important among these are homogeneous distribution of QDs throughout the host polymer,[18–20] material stability,[21,22] and the established cytotoxicity of many prototypical QDs.[22–24] If QDs are not uniformly distributed, variable material properties will likely result. Unstable QD dispersions will certainly have variable properties and even degrade under some application conditions. It is reasonable issues associated with uniformity and stability can be mitigated through direct bonding between the host polymer and the QD surface. Few examples of direct polymerization from the surface of archetypical CdSe QDs have appeared,[25] presumably because QDs and/or bonds tethering ligands to their surface are frequently not compatible with common polymerization conditions.[26] Fortunately, the ionic bonding of ligands with QD surfaces can undergo equilibrating exchange processes that allow introduction of various surface moieties, including polymers.[27–29] Another promising method for interfacing QDs with polymers relies upon exploiting the collective contributions of comparatively weak bonding interactions (e.g., van der Waals interactions) between surface groups on QDs and polymers.[30,31] This approach has provided tailoring QD solubility. Polymer coating can also slow, and even limit the release of cytotoxic ions, however this largely remains an outstanding challenge and clearly the most effective solution is to eliminate the use of cytotoxic elements.[24,32]

Recent synthetic advances have resulted in well-defined silicon nanocrystals (SiNCs) that have bettered the community's understanding of their properties and reactivity.[33–36] Modern SiNCs exhibit many, if not all of the favorable properties of traditional QDs with the added benefit of being non-toxic.[37–42] Their surface chemistry differs substantially from that of other QDs and is routinely tailored via various hydrosilylation approaches that afford robust covalent Si–C bonds.[43–47] These surface linkages preclude direct application of the surface exchange approach (vide supra). Approaches involving non-covalent surface-group/polymer interactions have been successfully applied to prepare SiNC/polymer hybrids typically with the intent of tailoring solubility.[48,49] As with other QDs, this strategy requires multiple synthetic steps to prepare the NC/polymer hybrid structure and the comparatively weak interactions between the polymer and nanoparticles could limit material stability. Alternative methods

Z. Yang, M. Dasog, A. R. Dobbie, Prof. J. G. C. Veinot
Department of Chemistry
University of Alberta
Edmonton, Alberta, T6G 2G2, Canada
E-mail: jveinot@ualberta.ca
R. Lockwood, Y. Zhi, Prof. A. Meldrum
Department of Physics
University of Alberta
Edmonton, Alberta, T6G 2G2, Canada

DOI: 10.1002/adfm.201302091

for interfacing SiNCs with polymers must be explored if hybrid materials with targeted properties are to be realized.

Investigations describing bulk silicon surface chemistry are vast and examples exist that offer a variety of promising approaches for interfacing SiNCs with polymers. Generally, modification of bulk silicon begins with a reactive surface (e.g., Si–H; Si–*X* where *X* = Cl, Br) that is subsequently modified by active functional groups on grafted molecules. For example: Tour and co-workers designed an efficient surface grafting approach on hydride-terminated silicon film surface using diazonium sources that leads to the formation of mono- and multilayers (i.e., oligomers and polymers).[50–52] Xu et al. investigated surface initiated atom transfer radical polymerization (ARTP) on Si surfaces derived from monolayer modification of hydride and halogen terminated silicon and effectively induced the formation of polymer brushes grafted surface.[53,54] Similarly, Zhang et al. reported a rapid grafting method to grow thick and dense polymer brushes on silicon using a multiple-step functionalization including UV-induced hydrosilylation followed by rare metal catalyzed polymerization.[55] All of these reports provide a basis for the preparation of SiNC/polymer hybrids, however many employ metal catalysts or reaction conditions that could compromise favorable SiNC properties.

Most reports of photochemically and thermally induced hydrosilylation are aimed at monolayer formation, however they also provide important platforms for controlled surface polymerization. Such "one-pot" hydrosilylation/polymerizations would dramatically simplify material preparation, minimize impurities, and assist in material processing. Our group, and others have reported polymerization of monomers (e.g., propionic acid) indicating catalyst free polymerization from SiNC surfaces is indeed possible.[56–58] Styrene has long been a preferred monolayer surface modification for SiNCs.[59] Polystyrene (PS) is a ubiquitous polymer with wide ranging applications. It has been introduced to bulk silicon surfaces via radical initiated polymerization,[60,61] and very recently thin films of PS composites containing ill-defined blue-emitting Si nanoparticles were investigated as an active material in prototype thin film transistors.[61]

To date, the bulk synthesis and processing of well-defined SiNC/PS hybrid materials have not been reported. Furthermore, demonstrations of micro and nanostructured SiNC/PS hybrid architectures exhibiting tunable photoluminescent properties have not appeared. Clearly, a comprehensive study on the physical and chemical properties as well as the solution processability of SiNC/PS hybrids would provide substantial benefit to the realization of functional materials and materials applications. To this end, we describe a systematic investigation of the preparation of a series of covalently linked SiNC/PS hybrids with tunable luminescence arising from state-of-the-art SiNCs that exhibit SiNC-based photoluminescence arising from quantum confinement. We also demonstrate the solution processability of the present SiNC/PS hybrids and prepare a variety of chemically resistant, uniform nano- and microscale photoluminescent architectures.

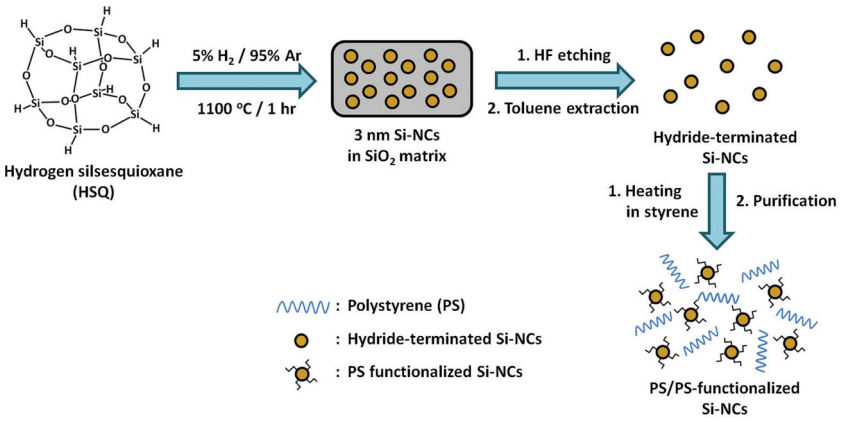

Scheme 1. Synthetic pathway from HSQ to polystyrene functionalized silicon nanocrystals/polystyrene hybrid material.

2. Results and Discussion

The methodology used to prepare the present SiNC/PS hybrids is summarized in **Scheme 1**. Well-defined SiNCs (i.e., d = 3, 5, and 8 nm) were prepared using a well-established procedure that exploits thermally induced disproportionation of commercially available hydrogen silsesquioxane (HSQ). Briefly, HSQ was heated in a slightly reducing atmosphere (i.e., 5% H_2/95% Ar) at 1100 °C to induce formation of SiNCs inside an SiO_2-like matrix. Larger SiNCs were obtained following a second processing of the composite obtained from this procedure at higher temperatures (i.e., 1200 °C, d = 5 nm; 1300 °C, d = 8 nm) in an Ar atmosphere.[62] The resulting brown solids were ground and etched using an ethanol/water HF solution to liberate hydride-terminated SiNCs.

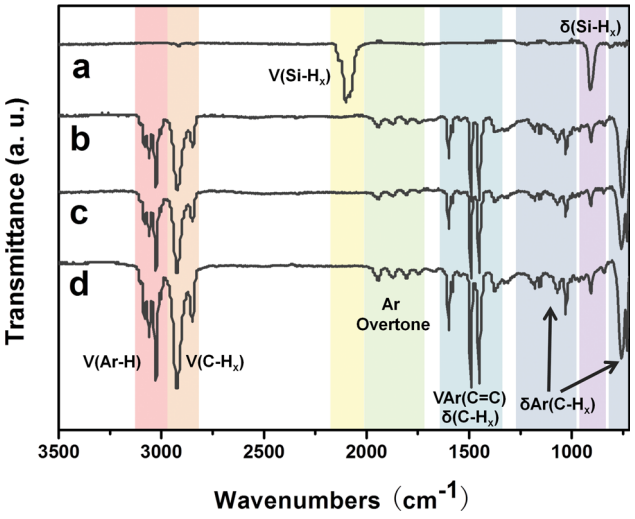

Figure 1. Fourier transform infrared (FT-IR) spectra of a) 3 nm hydride-terminated and b–d) Si nanocrystals with different sizes (b: 3 nm, c: 5 nm and d: 8 nm).

Subsequent functionalization/polymerization of styrene on the SiNC surfaces was achieved using a convenient "one-pot" procedure followed by purification. SiNCs were combined with a toluene solution of styrene and heated to 110 °C in an Ar atmosphere. Prolonged heating (i.e., at least 15 h) yielded an orange solution from which an amber solid was precipitated upon addition of ethanol. FT-IR spectroscopy of the products is consistent with SiNC surface functionalization and formation of polystyrene (**Figure 1**). Prior to reaction with styrene, the SiNC IR spectrum shows two distinctive signals at ≈2100 cm^{-1} and ≈850 cm^{-1} which are readily attributed to Si–H_x stretching and scissoring, respectively.[36] IR spectra of the SiNC/PS products are independent of the SiNC size and strongly resemble literature spectra of polystyrene.[63] We note C–H_x stretching bands attributable to the phenyl ring (3000–3200 cm^{-1}) and aliphatic polymer backbone (2650–2900 cm^{-1}). In addition, weak absorptions characteristic of overtone bands arising from mono-substituted aromatic rings are observed at 2000 cm^{-1} and 1650 cm^{-1}. Strong features at ≈1600 cm^{-1} and ≈1500 cm^{-1} are readily assigned to C=C stretching of the phenyl rings and a weak signal at *ca.* 1370 cm^{-1} is associated with C–H_x bending in aliphatic chain. The intense peak at ≈1450 cm^{-1} has also been attributed to the combination of phenyl group C=C stretching and aliphatic C–H_x bending.[63] Additional features, such as weak features between 1250 cm^{-1} and 1000 cm^{-1}, and strong peak at ≈760 cm^{-1} arise from in-plane and out-of-plane C–H_x bending. Of important note, there is no evidence of features arising from Si–H_x supporting the conclusion that SiNCs are covalently attached to the polystyrene. NMR analysis confirms no free styrene is present in purified samples (Figure S1, Supporting Information). Raman spectroscopy shows a clear absorption at 624 cm^{-1} confirming Si-C covalent linkages between polystyrene and the SiNC surface (Figure S2, Supporting Information).[64]

The uniformity of SiNC/PS hybrids was evaluated using bright field transmission electron microscopy (TEM). **Figure 2** shows minimal clustering of the SiNCs regardless of size indicating NCs are uniformly dispersed throughout the polymer. Photoluminescence spectroscopy clearly shows the size-dependent emission of SiNCs (i.e., d = 3 nm, λ_{em} = 700 nm; d = 5 nm, λ_{em} = 786 nm; d = 8 nm, λ_{em} = 888 nm) is preserved during functionalization (**Figure 3**). Consistent with this emission arising from a band gap transition, we note a radiative lifetime decay of 164.5 µs (Figure S3, Supporting Information) indicative of a SiNC-based band gap emission and no evidence of excitation wavelength dependence.

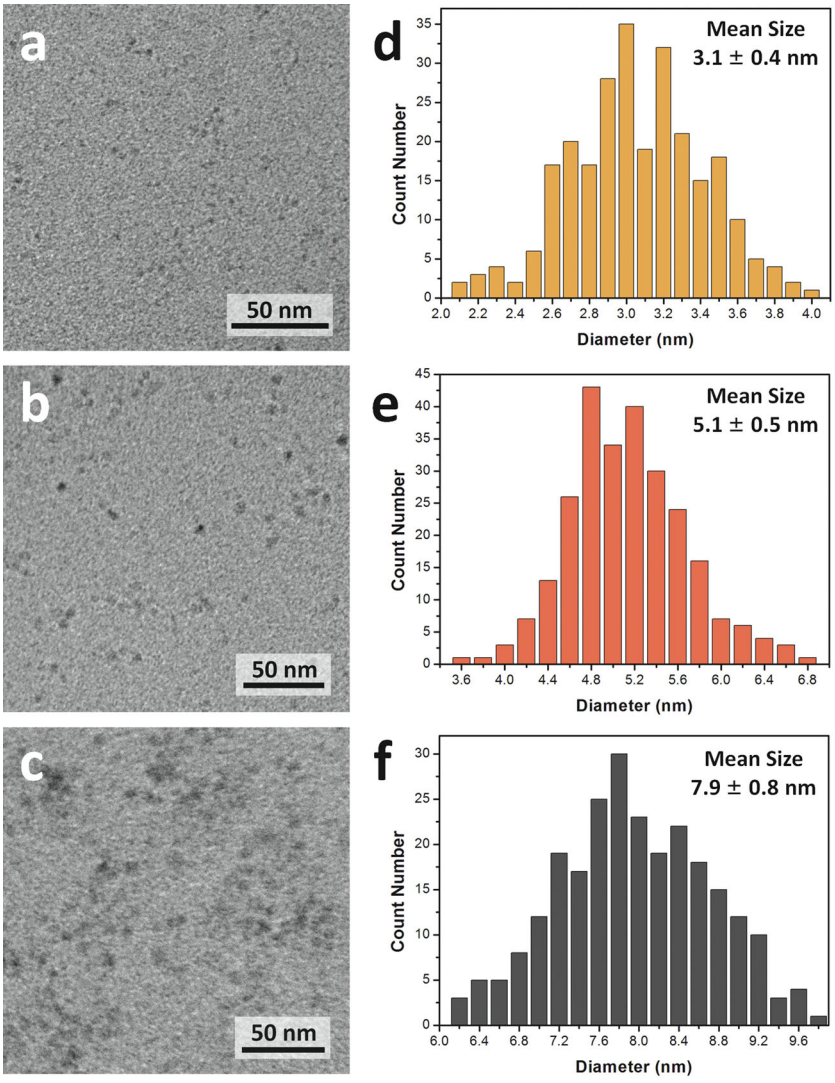

Figure 2. a–c) Bright field TEM images and d–f) size distribution of ensembles of polystyrene-functionalized silicon nanocrystals with several average diameters: a,d) 3.1 nm, b,e) 5.1 nm, and c,f) 7.9 nm.

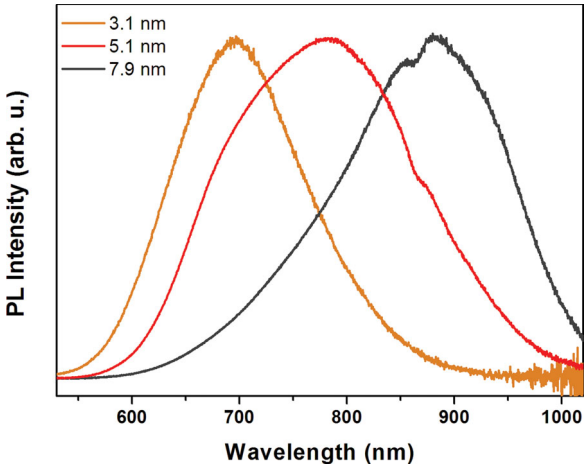

Figure 3. PL spectra of toluene solutions containing SiNC/PS hybrid materials with indicated mean particle sizes.

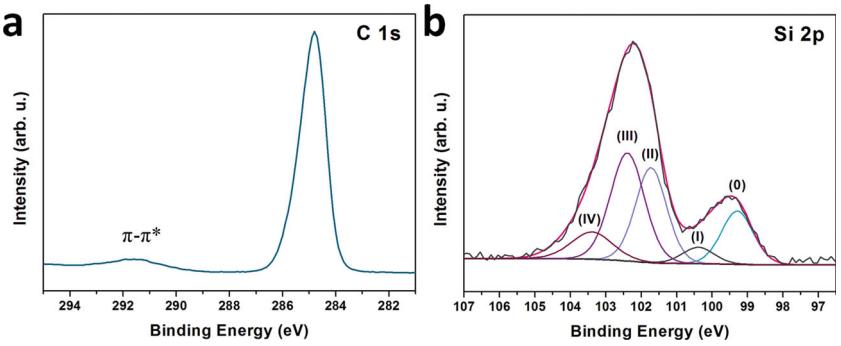

Figure 4. High-resolution XPS spectra of carbon (1s) and silicon (2p) for SiNCs/PS hybrid material. Fitting results are shown for the silicon spectrum with Si $2p_{3/2}$ signal shown. The Si $2p_{1/2}$ signals have omitted for clarity.

Survey X-ray photoelectron (XPS, not shown) and Energy Dispersive X-ray spectra (EDX) indicate the present SiNC/PS hybrids contain only silicon, oxygen and carbon. High-resolution XPS analyses further supports the formation of PS functionalized SiNCs. The C 1s emission located at 284.8 eV and a second emission at 291.6 eV (**Figure 4**a) substantiate the presence of aromatic groups (i.e., phenyl rings).[60] Multi-component features appear in Si 2p spectral region (Figure 4b). For clarity only the Si $2p_{3/2}$ components of the spin-orbit coupling pairs are displayed. Consistent with previous reports of functionalized SiNCs,[65] an emission attributable to elemental Si is noted at 99.3 eV. Other fitted features (i.e., 100.4, 101.6, 102.4 and 103.4 eV) are readily assigned to Si–C and silicon oxides.[57]

To investigate the impact of SiNC concentration on hybrid material properties, a series of materials were prepared using varied concentrations of 3 nm diameter SiNCs. The SiNC content was determined using thermal gravimetric analysis (TGA, Figure S4, Supporting Information). We note that in order to achieve complete SiNC functionalization, qualitatively determined by the formation of a non-opalescent solution, that longer processing times are required when more NCs are present (15 h for 0.8 wt% SiNCs, 59 h for 2.4 wt% SiNCs). The origin of this phenomenon is currently unclear and is the subject of ongoing investigation. Gel-permeation chromatography (GPC) provides molecular weight information for the SiNC/PS hybrids (Figures S5,S6, Supporting Information). Two major components are observed: a weak signal indicating a component with M_w several million g/mol and a second more intense peak is found at longer retention time corresponding to M_w = 200 000–330 000 g mol^{-1}. We tentatively attribute the larger molecular weight component to PS functionalized silicon particles, while those molecules with smaller M_w values are free PS formed during hydrosilylation.

As noted above, styrene has been a SiNC surface functionalization of choice because of the favorable solution properties and stability this surface modification endows. Surprisingly, reports of polymerization/oligomerization of styrene on/from the surface of SiNCs are rare.[61] Previously, styrene polymerization the presence of Si nanoparticles has been attributed to the homolytic cleavage of the Si-H bond.[61] While this reaction mechanism likely active at high reaction temperatures (i.e., ≥150 °C), there is little question it is not the dominant reaction pathway for the comparatively low temperatures reported here. **Scheme 2** illustrates how polymerization is expected to proceed. Rather than relying upon thermally induced homolytic cleavage of Si–H bond,[44] or the presence of an external radical initiator,[60] styrene can thermally self-initiate producing radicals via a Diels-Alder cycloaddition.[66] Besides the initiation of styrene polymerization in solution, these radicals can abstract hydrogen atoms from the Si–H terminated SiNC surface and the resulting silyl radicals are free to react with solution-phase styrene. This would form a Si–C bonds and new radicals localized on the beta-carbon of the surface bonded moiety which can subsequently react with more styrene to produce surface bonded oligomers/polymers or react in a surface chain-hydrosilylation reaction.[67] Finally reactions end with radical–radical termination events. A more detailed study of the polymerization mechanism and the roles of various additives are the subjects of ongoing investigations.

One of the primary goals of developing of functional hybrid materials like the SiNC/PS hybrids presented here is to effectively combine the characteristics of the constituent components. Photoluminescent response, solution processability, and chemical stability are key properties of the present systems. To demonstrate the unification and utility of these hybrid characteristics we describe the fabrication and properties of three photoluminescent prototype PS/SiNCs micro/nanostructures.

Photoluminescent optical fibres were fabricated upon by solution-coating of the interior surfaces of commercially available quartz capillaries. A toluene solution of the SiNC/PS (d = 3 nm) was drawn into a fiber that had been freed from its protective polyimide coating. Following evaporation of the solvent, a smooth thin film of the hybrid is formed on the inner capillary wall (see **Figure 5**). To approximate residual solvent content, TGA analysis of a thin film sample was performed indicated some toluene (ca. 8 mass %) remained (see Figure S7, Supporting Information). This solvent content exhibits no obvious influence on material properties. While the coating layer cannot be imaged directly with an optical microscope, intense uniform red PL couples the whole fiber under 488 argon laser irradiation (Figure 5f,g). Scanning electron microscopy (SEM) shows a smooth ≈1.5 μm thick polymer layer (Figure 5a–d).

To extend our solution coating procedure and fabricate nanoscaled structures it was necessary to determine if the present hybrids were resistant to the basic etching environment used to remove our nano-templates of choice (i.e., anodic aluminum oxide, AAO). This is particularly true considering hydride-terminated SiNCs are readily oxidized and their luminescence compromised upon exposure to basic solutions.[68] Reports also indicate the SiNC-based luminescence of hybrid materials decreases, is compromised or blue-shifts upon treatment with NH_4OH or NaOH solutions despite encapsulation.[69] To investigate resistance our hybrids to strongly basic conditions, samples were cast as transparent SiNC/PS luminescent thin films with thicknesses in the range of 45–60 μm (see **Figure 6**). These films were immersed for 15– and 30-day intervals in NaOH aqueous solutions (19.4 m) followed by evaluation of their morphology, texture, as well as the intense

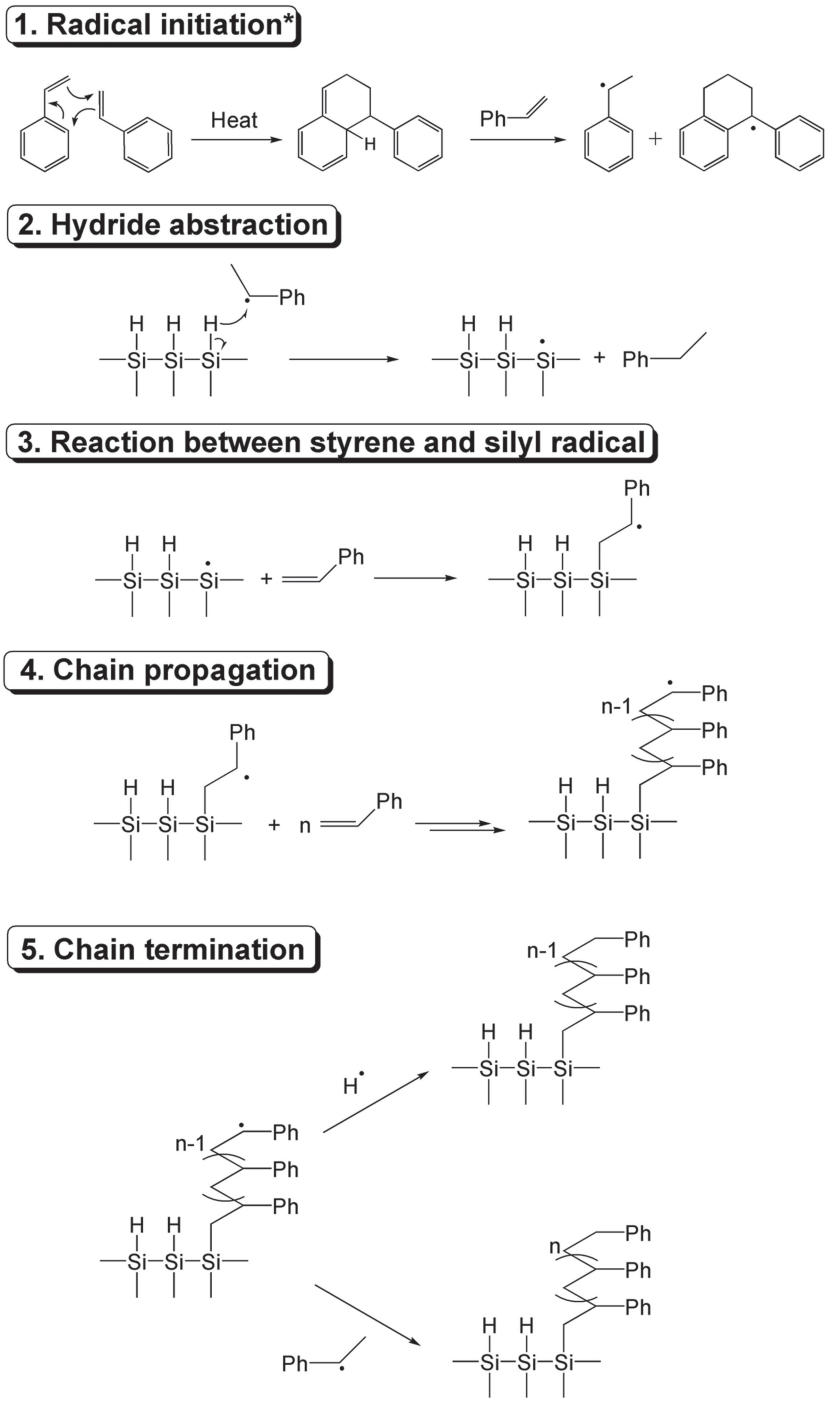

Scheme 2. Possible routes for the PS functionalization of hydride terminated silicon nanocrystals. Note (*) indicates multiple products co-exist during the initiation step.[66] Silicon surface radicals might also be created by the hydrogen transfer from the surface to ligand radical,[44] which is not shown here for clarity.

PL– negligible changes were detected (Figure 6a) in the optical response however some minor damage to the outer polymer surface was noted (Figure 6d). Freestanding thin films (i.e., thickness ≈500 nm) were also prepared via spincoating (see Figure S8, Supporting Information) and were exposed to saturated aqueous NaOH solutions for 7 days and not material degradation was detected at the sensitivity of SEM.

Having established our hybrids are chemically resistant, we endeavored to exploit their properties and fabricate hybrid nanostructures using a sacrificial template as summarized in Scheme S1, Supporting Information. Briefly, a piece of commercial available AAO bearing pore sizes in the range of d = 250–300 nm (Figure S9, Supporting Information) was dropcoated with a toluene solution of SiNC/PS (d = 3 nm). A glass slide was placed on top of the template and gently pressed resulting in a uniform thin film on top of the AAO. The hybrid solution was draw in the nanopore by capillary action. The solvent was evaporated upon standing in ambient conditions to yield a highly luminescent solid, film bearing hybrid nanofibers was obtained (see **Figure 7**). The established chemical resistance of the polystyrene component of the hybrid enabled basic etching of the AAO template without an detectable deterioration of SiNC optical response. Following template removal, no trace aluminum was detected at the sensitivity of the EDX technique consistent with complete template removal. SEM images of the liberated thin films clearly show bundles of flexible nanofibres with the diameter of ≈250 nm and lengths exceeding 30 µm (Figure 7c–f). The interface between the surface film layer and nanofibres is shown in Figure 7f. The thin film is ≈3 µm thick with smooth surface. On the interface we also notice the branch-like ends of the nanofibres that can be reasonably attributed to pore branching within the AAO template.

3. Conclusions

In summary, we have reported a straightforward synthetic route for preparing highly luminescent, solution processable SiNC/PS hybrid materials. Hydride-terminated SiNC surface have been surface modified with PS using size-independent radical-initiated hydrosilylation and detailed material information including, composition, optical properties and particle distribution, has been obtained. Combining the properties of SiNCs with PS significantly increases solubility rendering the particles solution processable and provides the opportunity to fabricate uniform nano- and microscale architectures. Furthermore, the polystyrene matrix renders SiNC chemically resistant to prolonged exposure to strongly basic conditions. Ongoing work will further investigate the fabrication of SiNCs hybrid materials with other functional polymers and co-polymers to understand the interaction

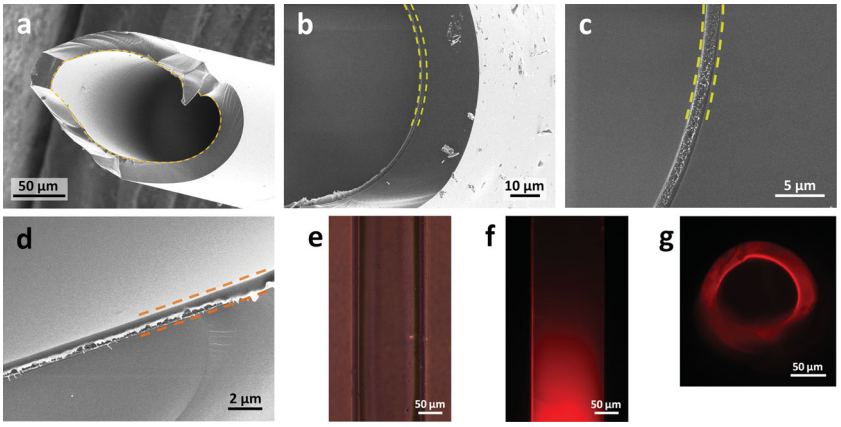

Figure 5. a–d) SEM images of optical fibers with 3 nm SiNC/PS coating on the inner wall. Dotted lines indicate the coating layer. e) Optical microscope and f,g) Fluorescence microscope images of the fibers with red emission from f) the top and g) cleaved end shown upon 488 nm excitation.

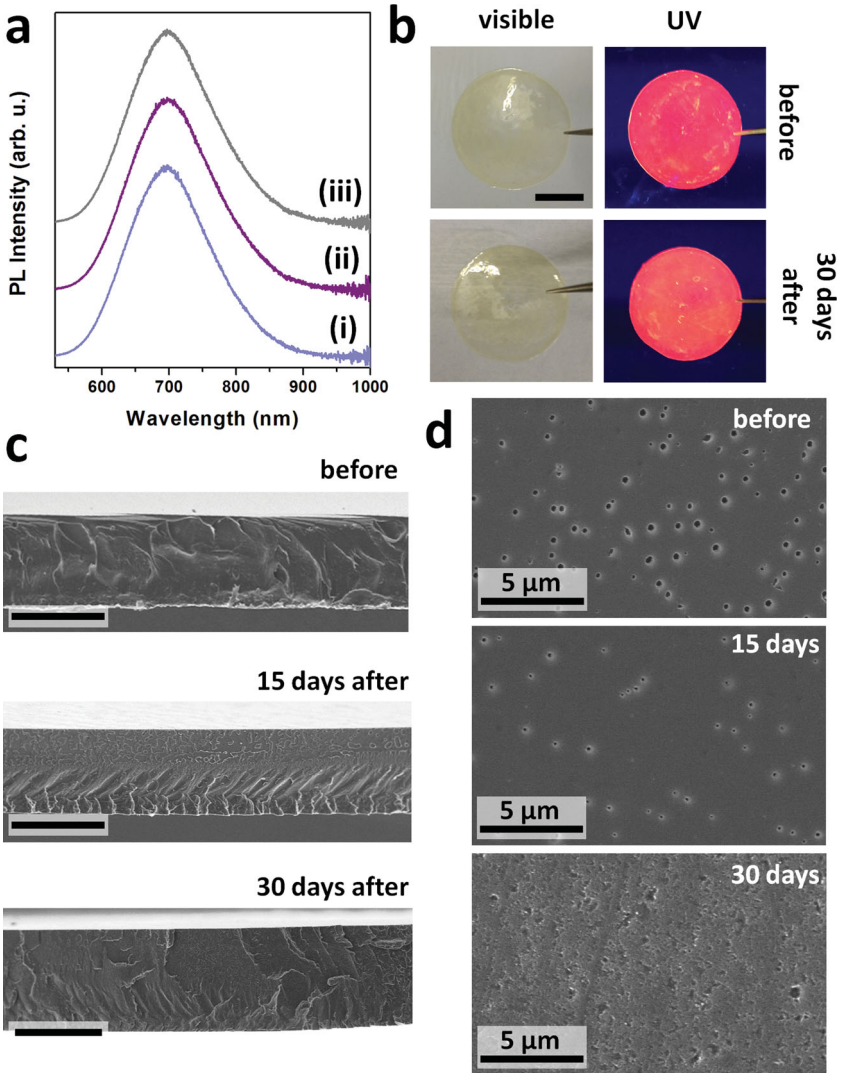

Figure 6. Characterizations of PS functionalized 3 nm SiNC/PS thin film before and after base solution resistance test. a) PL spectra and b) images showing their luminescent property before and after the test: i) before the test; ii) 15 days after, and iii) 30 days after (scale bar: 1 cm). c,d) SEM images of thin film before and after the immersion test (c) side view, d) top view, scale bar: 50 μm).

between SiNCs and conjugated polymers and further broaden their potential applications.

4. Experimental Section

Reagents and Materials: Hydrogen silsesquioxane (HSQ) was purchased from Dow Corning Corporation (Midland, MI) as FOx-17. Electronics grade hydrofluoric acid (HF, 49% aqueous solution) was purchased from J. T. Baker. Reagent grade methanol, toluene, and ethanol, as well as 1-dodecene (97%) and styrene (99%) were purchased from Sigma Aldrich and used as received. Styrene was purified by passing over neutral alumina immediately prior to use. Anodic aluminum oxide (AAO) membranes with 200 nm pores were obtained from Whatman.

Preparation of Oxide-Embedded SiNCs (3 nm): Established literature procedures were used to prepare oxide-embedded silicon nanocrystals ($SiNC/SiO_2$).[70] Briefly, solvent was removed from the stock HSQ solution under vacuum to yield a white solid. The solid (≈4 g) was placed in a quartz reaction boat and transferred to a Lindberg Blue tube furnace and heated from ambient to a peak processing temperature of 1100 °C at 18 °C min^{-1} in a slightly reducing atmosphere (5% H_2/95% Ar). The sample was maintained at the peak processing temperature for 1 h. Upon cooling to room temperature, the resulting amber solid was ground into a fine brown powder using a two-step process. The solid crushed using an agate mortar and pestle to remove large particles and finally ground to a fine powder using a Burrell Wrist Action Shaker upon shaking with high-purity silica beads for 5 hours. The resulting $SiNC/SiO_2$ powders were stable for extended periods and stored in standard glass vials.

Preparation of Oxide-Embedded SiNCs (d = 5 nm and 8 nm): After grinding with a mortar and pestle (vide supra), 0.5 g of $SiNC/SiO_2$ composite containing 3 nm SiNCs were transferred to a high temperature furnace (Sentro Tech Corp.) for further thermal processing in an inert argon atmosphere. This procedure leads to particle growth while maintaining relatively narrow particle size distributions. In the furnace, the $SiNC/SiO_2$ composite was heated to appropriate peak processing temperatures at 10 °C min^{-1} to achieve the target particle size (i.e., 1200 °C for 5 nm NCs and 1300 °C for 8 nm NCs). Samples were maintained at the peak processing temperature for 1 h. After cooling to room temperature, the brown composites were ground using procedures identical to those noted above.

Liberation of SiNCs: Hydride-terminated SiNCs were liberated from the $SiNC/SiO_2$ composite by HF etching. Predefined quantities of $SiNC/SiO_2$ composite corresponding to the final hybrid SiNC loading (i.e., 0.8, 1.6, and 2.4 wt% SiNC/polystyrene hybrids, 0.25 g, 0.50 g, and 1.0 g of ground $SiNC/SiO_2$, respectively) were transferred to a polyethylene terephthalate beaker equipped with a Teflon coated stir bar. Ethanol (3 mL) and water (3 mL) were added under mechanical stirring to form a brown suspension followed by 3 mL of 49% HF aqueous solution (Caution! HF must be

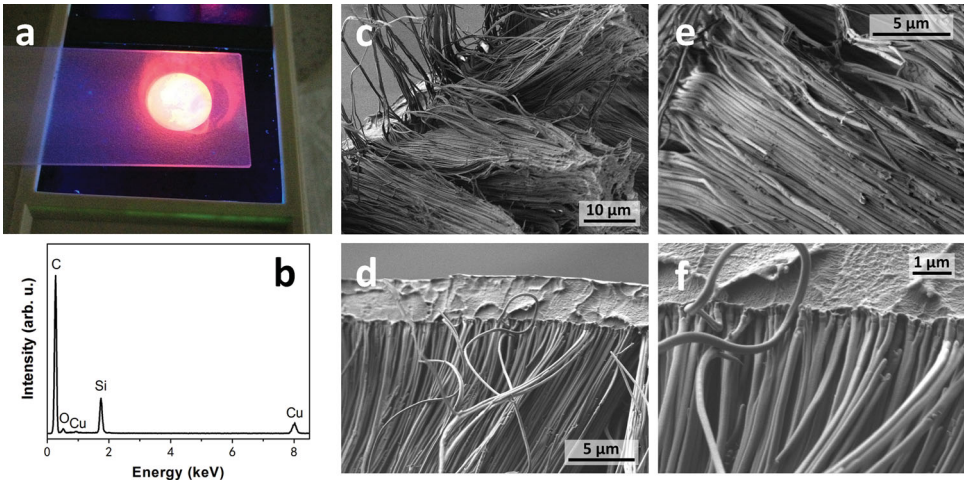

Figure 7. a) Luminescent nanofibres fabricated by 3 nm SiNC/PS hybrid material by facile drop-casting approach. b) EDX showing the existence of silicon, carbon and oxygen signals. Cu signals arise from the sample grid. c–f) SEM images of nanofibres liberated from the template.

handled with extreme care). After 1 h of etching in subdued light the suspension appeared orange/yellow. Hydride-terminated SiNCs were subsequently extracted from the aqueous layer into ≈30 mL of toluene by multiple (i.e., 3 × 10 mL) extractions. The SiNC toluene suspension was transferred to test tubes and the SiNCs were isolated by centrifugation at 3000 rpm.

Formation SiNC/Polystyrene Hybrids: After decanting the clear toluene supernatant, hydride-terminated SiNCs were dispersed in 12 mL of a 1:1 styrene:toluene mixture to yield a cloudy suspension that was transferred to a dry 100 mL Schlenk flask equipped with magnetic stir bar and attached to an argon charged Schlenk line. The reaction mixture was subjected to three freeze–pump–thaw cycles and finally backfilled with argon. The temperature was increased to 110 °C in an oil bath under a static argon atmosphere. The reaction mixture was stirred for a minimum of 15 h to yield a transparent orange solution.

Following cooling to room temperature, equal volumes of the orange solution were dispensed into 4 test tubes and 10 mL of ethanol was added yielding a cloudy light yellow dispersion. The precipitate was isolated by centrifugation at 3000 rpm for 10 min. The supernatant was decanted and the precipitate was redispersed in a minimum amount (≈5 mL) of toluene with ultrasonication for 0.5 h and subsequently reprecipitated by addition of ethanol. This dissolution/precipitation/centrifugation procedure was repeated twice. Finally, the purified hybrid material were redispersed in toluene, filtered through a 0.45 µm PTFE syringe filter and dried under vacuum for 12 h to yield an amber solid that was stored in vial for further use.

Fabrication of Polystyrene/SiNC Coated Fibers: Polyimide coated fused-silica capillary tubing was purchased from Polymicro Technologies with a 102 µm inner diameter (ID) and a 164 µm outer diameter (OD). Tubing was cleaved into ca. 5 cm long pieces, placed in a quartz boat and transferred into a tube furnace (Barnstead Thermolyne 21100). The tube was evacuated with a roughing pump and backfilled with oxygen, then heated at 650 °C for 45 min under a steady flow of oxygen to remove the polyimide cladding layer. After cooling to room temperature, fibers were stored in air in a covered plastic petri dish for further use.

Coating of the internal surface of the capillaries was achieved by dissolving 0.2 g of the 2.4 wt% SiNC (d = 3 nm)/polystyrene hybrid in ≈3 mL of toluene. The end of the capillary was dipped into the toluene solution causing it to be drawn into the tube by capillary action. The fibers were subsequently placed perpendicularly in a glass vial and dried in the air at room temperature for 24 h.

Fabrication of SiNC/Polystyrene Nanofibres: Anodic aluminum oxide (AAO) membranes were placed on a standard glass microscope slide. 0.1 g of 0.8 wt% SiNC(d = 3 nm)/polystyrene hybrid was dissolved in 3 mL of toluene and a predefined volume (i.e., 60 µL) of the solution was drop-cast using a micropipette onto the top surface of the AAO. A second glass slide was placed on top of the liquid and gently pressed to form a "glass-liquid-AAO-glass" assembly. After drying in the air, the glass slides were removed and the coated AAO was immersed in 10 M aqueous KOH for 24 h to remove the AAO template. The resulting transparent film was washed with deionized water and ethanol and finally dried in the air at room temperature for 24 h.

Fabrication and Stability of Freestanding SiNC/Polystyrene Thin Films: The toluene solution (700 µL) used for AAO templated nanofiber preparation (vide supra) was dropped into the wells of a glass spot plate. The solvent was evaporated after 15-h in air at atmospheric pressure resulting in a curved thin film that was readily released from the glass surface. The chemical resistance of the thin films was assessed by immersing it in a saturated NaOH solution for a predefined time (i.e., 15 days and 30 days) after which the photoluminescence (PL) was evaluated. Before evaluation of PL response, samples were rinsed with deionized water and ethanol, and dried in vacuum for 24 h. For the fabrication of 500 nm-thick thin film, ≈25 µL of the toluene solution used for AAO templated nanofiber preparation was transferred onto a clean silicon wafer (1.5 cm × 1.5 cm) and spin-coated for 3 times with the speed of 3000 rpm for 30 s. Then the thin film with the substrate was soaked in saturated NaOH solution for 7 days. Finally the thin film was taken out and rinsed with deionized water and ethanol, and dried in vacuum for 24 h before SEM measurement.

Material Characterization and Instrumentation: PL spectra were obtained upon irradiating a quartz vial containing a toluene solution of the sample in question with the 441 nm line of a GaN laser. Emitted photons were collected with a fiber optic connected to an Ocean Optics USB2000 spectrometer. The spectrometer spectral response was normalized using a black body radiator. ^{1}H NMR spectra were recorded on an Agilent/Varian INova four-channel 500 MHz spectrometer and referenced externally to $SiMe_4$. FT-IR spectroscopy was performed on uniform powder samples using a Nicolet Magna 750 IR spectrophotometer. Raman spectroscopy was performed using a Renishaw inVia Raman microscope equipped with a 514 nm diode laser on the sample. GPC was performed at 35 °C using THF (stablised with 250 ppm BHT) as the eluent at a flow rate of 1 mL min^{-1}. GPC measurements were made using a Varian GMBH GPC50 instrument and calibrated to polystyrene standards.

X-ray photoelectron spectroscopy was acquired in energy spectrum mode at 210 W, using a Kratos Axis Ultra X-ray photoelectron spectrometer. Samples were prepared as films drop-cast from solution onto a copper foil substrate. CasaXPS (Vamas) software was used to process high-resolution spectra. All spectra were calibrated to the C1s

emission (284.8 eV) arising from adventitious carbon. After calibration, the extrinsic loss structure in the background from each spectrum was subtracted using a Shirley-type background. Sample compositions were determined from the emission intensities of the survey spectra using appropriate sensitivity factors. The high-resolution Si 2p region of spectra were fit to Si $2p_{1/2}$/Si $2p_{3/2}$ partner lines, with spin-orbit splitting fixed at 0.6 eV, and the Si $2p_{1/2}$/Si $2p_{3/2}$ intensity ratio was set to 1/2.

Thermal gravimetric analysis was performed using a Perkin-Elmer Pyris 1 TGA. Samples were heated in a Pt pan under N_2 gas from 20 to 900 °C at a rate of 10 °C min^{-1}.

Transmission electron microscopy and energy dispersive X-ray (EDX) analyses were performed using a JEOL-2010 (LaB_6 filament) electron microscope with an accelerating voltage of 200 keV. TEM samples of SiNCs were drop-casted onto a holey carbon coated copper grid (SPI supplies) and the solvent was evaporated in vacuum. Secondary electron scanning electron microscopy images of the nanofibres were obtained using field-emission SEM (JEOL JSM 7500F) with an accelerating voltage of 0.5 to 1.0 kV. Optical fibers and thin films were imaged using JEOL 6301F field-emission SEM with an acceleration voltage of 5 kV. TEM and SEM images were processed using ImageJ software (NIH). Particle size distribution was processed by visual analysis of the images aided by ImageJ software.

For the fluorescent imaging of the polymer-coated capillaries, an Ar^+ laser (λ = 488 nm) was applied at a pumping power of 300 mW. The beam was incident in free space through the side of the optical fiber, which was placed on the stage of an epifluorescence microscope. The resulting fluorescence was collected through a 10× microscope objective (numerical aperture of 0.22) and imaged using a color CCD camera (Fast 1394 FireWire, Retiga EX).

Supporting Information

Supporting Information is available from the Wiley Online Library or from the author.

Acknowledgements

The authors acknowledge funding from the Natural Sciences and Engineering Research Council of Canada (NSERC), Canada Foundation for Innovation (CFI), Alberta Science and Research Investment Program (ASRIP), Alberta Innovates Technology Futures (AITF), and University of Alberta Department of Chemistry. The Meldrum Team thanks NSERC and AITF for financial support. The authors would like to thank W. C. Moffat, M. Skjel, M. Hoyle, and V. Bretzler (Technische Universität München, TUM) for assistance with FT-IR spectroscopy and TGA analysis. The staff at the Alberta Centre for Surface Engineering and Sciences (ACSES) is thanked for XPS analysis. G. Braybrook, K. Rodewald (TUM) and G. Popowich are thanked for assistance with SEM and TEM. Dr. F. Deubel (TUM) and Prof. Dr. B. Rieger (TUM) are thanked for GPC analysis and valuable suggestions. All Veinot Team members are also thanked for useful discussion.

Received: June 19, 2013
Revised: August 13, 2013
Published online: October 14, 2013

[1] C. Burda, X. Chen, R. Narayanan, M. A. El-Sayed, *Chem. Rev.* **2005**, *105*, 1025.
[2] X. Michalet, F. F. Pinaud, L. A. Bentolila, J. M. Tsay, S. Doose, J. J. Li, G. Sundaresan, A. M. Wu, S. S. Gambhir, S. Weiss, *Science* **2005**, *307*, 538.
[3] P. V. Kamat, *J. Phys. Chem. C* **2007**, *111*, 2834.
[4] X. Gao, Y. Cui, R. M. Levenson, L. W. K. Chung, S. Nie, *Nat. Biotechnol.* **2004**, *22*, 969.
[5] C. B. Murray, D. J. Norris, M. G. Bawendi, *J. Am. Chem. Soc.* **1993**, *115*, 8706.
[6] R. D. Schaller, V. I. Klimov, *Phys. Rev. Lett.* **2004**, *92*, 186601.
[7] Z. A. Peng, X. Peng, *J. Am. Chem. Soc.* **2000**, *123*, 183.
[8] X. Peng, M. C. Schlamp, A. V. Kadavanich, A. P. Alivisatos, *J. Am. Chem. Soc.* **1997**, *119*, 7019.
[9] B. O. Dabbousi, M. G. Bawendi, O. Onitsuka, M. F. Rubner, *Appl. Phys. Lett.* **1995**, *66*, 1316.
[10] J. Lee, V. C. Sundar, J. R. Heine, M. G. Bawendi, K. F. Jensen, *Adv. Mater.* **2000**, *12*, 1102.
[11] L. Bakueva, S. Musikhin, M. A. Hines, T. W. F. Chang, M. Tzolov, G. D. Scholes, E. H. Sargent, *Appl. Phys. Lett.* **2003**, *82*, 2895.
[12] D. Y. Lee, J. T. Pham, J. Lawrence, C. H. Lee, C. Parkos, T. Emrick, A. J. Crosby, *Adv. Mater.* **2013**, *25*, 1248.
[13] Y.-H. Chan, F. Ye, M. E. Gallina, X. Zhang, Y. Jin, I. C. Wu, D. T. Chiu, *J. Am. Chem. Soc.* **2012**, *134*, 7309.
[14] G. B. Sukhorukov, A. L. Rogach, M. Garstka, S. Springer, W. J. Parak, A. Muñoz-Javier, O. Kreft, A. G. Skirtach, A. S. Susha, Y. Ramaye, R. Palankar, M. Winterhalter, *Small* **2007**, *3*, 944.
[15] R. Freeman, T. Finder, L. Bahshi, R. Gill, I. Willner, *Adv. Mater.* **2012**, *24*, 6416.
[16] S. Ren, L.-Y. Chang, S.-K. Lim, J. Zhao, M. Smith, N. Zhao, V. Bulović, M. Bawendi, S. Gradečak, *Nano Lett.* **2011**, *11*, 3998.
[17] X. Li, C. Bullen, J. W. M. Chon, R. A. Evans, M. Gu, *Appl. Phys. Lett.* **2007**, *90*, 161116.
[18] R. A. Vaia, H. D. Wagner, *Mater. Today* **2004**, *7*, 32.
[19] M. Bradley, N. Bruno, B. Vincent, *Langmuir* **2005**, *21*, 2750.
[20] N. Joumaa, M. Lansalot, A. Théretz, A. Elaissari, A. Sukhanova, M. Artemyev, I. Nabiev, J. H. M. Cohen, *Langmuir* **2006**, *22*, 1810.
[21] J. Tang, L. Brzozowski, D. A. R. Barkhouse, X. Wang, R. Debnath, R. Wolowiec, E. Palmiano, L. Levina, A. G. Pattantyus-Abraham, D. Jamakosmanovic, E. H. Sargent, *ACS Nano* **2010**, *4*, 869.
[22] A. M. Derfus, W. C. W. Chan, S. N. Bhatia, *Nano Lett.* **2003**, *4*, 11.
[23] G. Oberdorster, E. Oberdorster, J. Oberdorster, *Environ. Heatlth Perspect.* **2005**, *113*, 823.
[24] U. Resch-Genger, M. Grabolle, S. Cavaliere-Jaricot, R. Nitschke, T. Nann, *Nat. Methods* **2008**, *5*, 763.
[25] T. Nakashima, T. Sakakibara, T. Kawai, *Chem. Lett.* **2005**, *34*, 1410.
[26] N. Tomczak, D. Jańczewski, M. Han, G. J. Vancso, *Prog. Polym. Sci.* **2009**, *34*, 393.
[27] Y. A. Wang, J. J. Li, H. Chen, X. Peng, *J. Am. Chem. Soc.* **2002**, *124*, 2293.
[28] M. Wang, T. E. Dykstra, X. Lou, M. R. Salvador, G. D. Scholes, M. A. Winnik, *Angew. Chem. Int. Ed.* **2006**, *45*, 2221.
[29] K. Sill, T. Emrick, *Chem. Mater.* **2004**, *16*, 1240.
[30] T. Pellegrino, L. Manna, S. Kudera, T. Liedl, D. Koktysh, A. L. Rogach, S. Keller, J. Rädler, G. Natile, W. J. Parak, *Nano Lett.* **2004**, *4*, 703.
[31] W. W. Yu, E. Chang, J. C. Falkner, J. Zhang, A. M. Al-Somali, C. M. Sayes, J. Johns, R. Drezek, V. L. Colvin, *J. Am. Chem. Soc.* **2007**, *129*, 2871.
[32] T. C. King-Heiden, P. N. Wiecinski, A. N. Mangham, K. M. Metz, D. Nesbit, J. A. Pedersen, R. J. Hamers, W. Heideman, R. E. Peterson, *Environ. Sci. Technol.* **2009**, *43*, 1605.
[33] J. A. Kelly, A. M. Shukaliak, M. D. Fleischauer, J. G. C. Veinot, *J. Am. Chem. Soc.* **2011**, *133*, 9564.
[34] D. C. Hannah, J. Yang, P. Podsiadlo, M. K. Y. Chan, A. Demortière, D. J. Gosztola, V. B. Prakapenka, G. C. Schatz, U. Kortshagen, R. D. Schaller, *Nano Lett.* **2012**, *12*, 4200.
[35] J. B. Miller, A. R. Van Sickle, R. J. Anthony, D. M. Kroll, U. R. Kortshagen, E. K. Hobbie, *ACS Nano* **2012**, *6*, 7389.

[36] M. Dasog, Z. Yang, S. Regli, T. M. Atkins, A. Faramus, M. P. Singh, E. Muthuswamy, S. M. Kauzlarich, R. D. Tilley, J. G. C. Veinot, *ACS Nano* **2013**, *7*, 2676.
[37] N. H. Alsharif, C. E. M. Berger, S. S. Varanasi, Y. Chao, B. R. Horrocks, H. K. Datta, *Small* **2009**, *5*, 221.
[38] F. Erogbogbo, K.-T. Yong, I. Roy, G. Xu, P. N. Prasad, M. T. Swihart, *ACS Nano* **2008**, *2*, 873.
[39] J.-H. Park, L. Gu, G. von Maltzahn, E. Ruoslahti, S. N. Bhatia, M. J. Sailor, *Nat. Mater.* **2009**, *8*, 331.
[40] L. Pavesi, L. Dal Negro, C. Mazzoleni, G. Franzo, F. Priolo, *Nature* **2000**, *408*, 440.
[41] Z. C. Holman, C.-Y. Liu, U. R. Kortshagen, *Nano Lett.* **2010**, *10*, 2661.
[42] C.-Y. Liu, Z. C. Holman, U. R. Kortshagen, *Nano Lett.* **2008**, *9*, 449.
[43] M. Rosso-Vasic, E. Spruijt, Z. Popovic, K. Overgaag, B. van Lagen, B. Grandidier, D. Vanmaekelbergh, D. Dominguez-Gutierrez, L. De Cola, H. Zuilhof, *J. Mater. Chem.* **2009**, *19*, 5926.
[44] J. M. Buriak, *Chem. Rev.* **2002**, *102*, 1271.
[45] S. Ciampi, J. B. Harper, J. J. Gooding, *Chem. Soc. Rev.* **2010**, *39*, 2158.
[46] J. G. C. Veinot, *Chem. Commun.* **2006**, *0*, 4160.
[47] X. Li, Y. He, M. T. Swihart, *Langmuir* **2004**, *20*, 4720.
[48] C. M. Hessel, M. R. Rasch, J. L. Hueso, B. W. Goodfellow, V. A. Akhavan, P. Puvanakrishnan, J. W. Tunnel, B. A. Korgel, *Small* **2010**, *6*, 2026.
[49] F. Erogbogbo, K.-T. Yong, I. Roy, R. Hu, W.-C. Law, W. Zhao, H. Ding, F. Wu, R. Kumar, M. T. Swihart, P. N. Prasad, *ACS Nano* **2010**, *5*, 413.
[50] B. Chen, A. K. Flatt, H. Jian, J. L. Hudson, J. M. Tour, *Chem. Mater.* **2005**, *17*, 4832.
[51] M. Lu, W. M. Nolte, T. He, D. A. Corley, J. M. Tour, *Chem. Mater.* **2009**, *21*, 442.
[52] T. He, H. Ding, N. Peor, M. Lu, D. A. Corley, B. Chen, Y. Ofir, Y. Gao, S. Yitzchaik, J. M. Tour, *J. Am. Chem. Soc.* **2008**, *130*, 1699.
[53] F. J. Xu, Z. L. Yuan, E. T. Kang, K. G. Neoh, *Langmuir* **2004**, *20*, 8200.
[54] F. J. Xu, Q. J. Cai, E. T. Kang, K. G. Neoh, *Langmuir* **2005**, *21*, 3221.
[55] N. Zhang, S. Salzinger, F. Deubel, R. Jordan, B. Rieger, *J. Am. Chem. Soc.* **2012**, *134*, 7333.
[56] Z. F. Li, E. Ruckenstein, *Nano Lett.* **2004**, *4*, 1463.
[57] R. J. Clark, M. K. M. Dang, J. G. C. Veinot, *Langmuir* **2011**, *27*, 2073.
[58] F. Deubel, M. Steenackers, J. A. Garrido, M. Stutzmann, R. Jordan, *Macromol. Mater. Eng.* **2013**, DOI: 10.1002/mame.201200392.
[59] F. Hua, M. T. Swihart, E. Ruckenstein, *Langmuir* **2005**, *21*, 6054.
[60] I. W. Moran, K. R. Carter, *Langmuir* **2009**, *25*, 9232.
[61] M. X. Dung, J.-K. Choi, H.-D. Jeong, *ACS Appl. Mater. Interfaces* **2013**, *5*, 2400.
[62] C. M. Hessel, D. Reid, M. G. Panthani, M. R. Rasch, B. W. Goodfellow, J. Wei, H. Fujii, V. Akhavan, B. A. Korgel, *Chem. Mater.* **2011**, *24*, 393.
[63] C. Y. Liang, S. Krimm, *J. Polym. Sci.* **1958**, *27*, 241.
[64] D. Lin-Vien, N. B. Colthup, W. G. Fateley, J. G. Grasselli, in *The handbook of infrared and raman characteristic frequencies of organic molecules*, Academic Press, San Diego **1991**, p. 251.
[65] C. M. Hessel, E. J. Henderson, J. A. Kelly, R. G. Cavell, T.-K. Sham, J. G. C. Veinot, *J. Phys. Chem. C* **2008**, *112*, 14247.
[66] K. S. Khuong, W. H. Jones, W. A. Pryor, K. N. Houk, *J. Am. Chem. Soc.* **2005**, *127*, 1265.
[67] R. L. Cicero, M. R. Linford, C. E. D. Chidsey, *Langmuir* **2000**, *16*, 5688.
[68] S. Regli, J. A. Kelly, J. G. C. Veinot, *MRS Symp. Proc.* **2011**, *1359*.
[69] Z. F. Li, M. T. Swihart, E. Ruckenstein, *Langmuir* **2004**, *20*, 1963.
[70] C. M. Hessel, E. J. Henderson, J. G. C. Veinot, *Chem. Mater.* **2006**, *18*, 6139.